Studying *in vivo* dynamics of xylem-transported $^{11}CO_2$ using positron emission tomography

Jens Mincke[1,2,*], Jan Courtyn[3], Christian Vanhove[2], Stefaan Vandenberghe[2], Kathy Steppe[1]

[1] Laboratory of Plant Ecology, Department of Plants and Crops, Faculty of Bioscience Engineering, Ghent University, Ghent, Belgium

[2] MEDISIP - INFINITY, Department of Electronics and Information Systems, Faculty of Engineering and Architecture, Ghent University, Ghent, Belgium

[3] Medical Molecular Imaging and Therapy, Department of Radiology and Nuclear Medicine, Ghent University Hospital, Ghent, Belgium

[*]Corresponding author:

Dr. Jens Mincke

E-mail: Jens.Mincke@UGent.be; kathy.steppe@UGent.be

Postal address: Coupure links 653, 9000 Ghent, Belgium

Word count:

- Introduction: 1011
- Main body: 6291
- Materials and Methods: 2982
- Results: 473
- Discussion: 1825
- Figures: 8
- Tables: 1

Abstract

Respired CO_2 in woody tissues can build up in the xylem and dissolve in the sap solution to be transported through the plant. From the sap, a fraction of the CO_2 can either radially diffuse to the atmosphere or be assimilated in chloroplasts present in woody tissues. These processes occur simultaneously in stems and branches making it difficult to study their specific dynamics. Therefore, an ^{11}C-enriched aqueous solution was administered to young branches of *Populus tremula* L., which were subsequently imaged by positron emission tomography (PET). This approach allows *in vivo* visualisation of the internal movement of CO_2 inside branches at high spatial and temporal resolution, and enables direct measurement of the transport speed of xylem-transported CO_2 (v_{CO2}). Through compartmental modelling of the dynamic data obtained from the PET images we (i) quantified v_{CO2} and (ii) proposed a new method to assess the fate of xylem-transported $^{11}CO_2$ within the branches. It was found that a fraction of 0.49 min^{-1} of CO_2 present in the xylem was transported upwards. A fraction of 0.38 min^{-1} diffused radially from the sap to the surrounding parenchyma and apoplastic spaces ($CO_{2,PA}$) to be assimilated by woody tissue photosynthesis. Another 0.12 min^{-1} of the xylem-transported CO_2 diffused to the atmosphere via efflux. The remaining CO_2 (i.e. 0.01 min^{-1}) was stored as $CO_{2,PA}$, representing the build-up within parenchyma and apoplastic spaces to be assimilated or directed to the atmosphere. Here, we demonstrate the outstanding potential of $^{11}CO_2$-based plant-PET in combination with compartmental modelling to advance our understanding of internal CO_2 movement and the respiratory physiology within woody tissues.

Key words: $^{11}CO_2$, carbon-11 (^{11}C), CO_2 recycling, CO_2 refixation, plant-PET, radial CO_2 diffusion, stem photosynthesis, stem respiration, woody tissue photosynthesis, xylem CO_2 transport

Introduction

During cell respiration, carbon substrates are oxidized in mitochondria which releases CO_2 as a by-product. Outer tissues of the stem present substantial barriers to radial CO_2 diffusion (Steppe *et al.* 2007), so that locally respired CO_2 builds up in the xylem and dissolves in the sap solution while reaching a substantially higher concentration (often between 3 and 10 %, and sometimes up to 26 %, reviewed by Teskey *et al.* 2008) than that in the atmosphere (*c.* 0.04 %). Xylem CO_2 concentration ($[CO_2]$) in the gaseous phase is hereby in equilibrium with CO_2 species (CO_2 (aq), HCO_3^- and CO_3^{2-}) dissolved in the sap solution (sap $[CO_2^*]$) (Hari *et al.* 1991; Levy *et al.* 1999; McGuire & Teskey 2004). Upon dissolution in xylem sap, CO_2 is transported upward with the transpiration stream throughout the plant (Stringer & Kimmerer 1993). Part of the internally transported CO_2 (F_T) (see Table 1 for a list of abbreviations) can diffuse to surrounding xylem and phloem parenchyma and apoplastic spaces ($CO_{2,PA}$ in Fig. 1) from where it has two main pathways: it can either radially diffuse into the atmosphere via stem CO_2 efflux (E_A) which is facilitated by the $[CO_2]$ gradient across the xylem – atmosphere (Teskey *et al.* 2008) or be assimilated (A_X) in chloroplasts present in the bark, xylem rays, and pith tissues (van Cleve *et al.* 1993; Berveiller *et al.* 2007; Pfanz 2008; Rentzou & Psaras 2008; Bloemen *et al.* 2016). This latter process will be referred to as woody tissue photosynthesis (P_{wt}), which is a recycling mechanism that has been shown to contribute to the total carbon budget of plants (Saveyn *et al.* 2010; Ávila *et al.* 2014). The remaining fraction of CO_2 is stored (ΔS) and can be regarded as build-up of $CO_{2,PA}$ that is to be assimilated or directed to the atmosphere. A schematic representation of these CO_2 fluxes in woody plants is given in Fig. 1.

Our understanding of xylem-transported CO_2 in relation to plant respiration is less advanced than our knowledge of water transport or photosynthesis (Amthor 2000; Atkin & Macherel 2009; Thornley 2011), although progress has been made. Specifically, the classic

assumption of E_A being a measure of local stem respiration (R_S) has been refuted as it has been demonstrated that part of the respired CO_2 dissolves in the sap solution to be transported upward through the xylem tissue (Hari *et al.* 1991; Levy *et al.* 1999; Teskey *et al.* 2008, 2017; Höltta & Kolari 2009; Angert *et al.* 2012). However, questions about the transport of respired CO_2 through the xylem (F_T) still remain, as it confounds interpretation of CO_2 efflux measurements from soil (Aubrey & Teskey 2009) and leaves (Stutz *et al.* 2017; Stutz & Hanson 2019), and it supports the mechanism of internal CO_2 recycling by P_{wt} (Bloemen *et al.* 2013a). It is expected that assimilation of xylem-transported CO_2 via P_{wt} is important for plant functioning, especially for young plant structures as well as under drought stress conditions (Cernusak & Marshall 2000; Bloemen *et al.* 2013a; Cernusak & Cheesman 2015; Steppe *et al.* 2015; Vandegehuchte *et al.* 2015). However, methodological constraints to study internal CO_2 transport (F_T) in woody tissues hinder accurate estimates of its dynamic fate (Teskey *et al.* 2008). Quantification of F_T is not straightforward, especially in relation to stem respiration, and two methods are described (McGuire & Teskey 2004; Angert *et al.* 2012; Salomón *et al.* 2018, 2019a). A mass balance approach has been proposed (on a volume basis; µmol CO_2 m^{-3} s^{-1}) to account for F_T in R_S estimates:

$$R_S = F_T + E_A + \Delta S \qquad (1)$$

$$= \frac{F_{H2O}}{V} \times \Delta[CO_2^*] + \frac{f_{air}}{V} \times \Delta[CO_2] + \frac{L}{T} \times \Delta[CO_2^*]_T$$

where ΔS is the storage CO_2 flux and excludes P_{wt} (McGuire & Teskey 2004). In this approach, gas exchange measurements are performed on a stem segment enclosed in a cuvette in addition to measurements of sap flow F_{H2O} (L s^{-1}), sapwood volume V within the enclosed stem segment (m^3), sap [CO_2^*] at top and bottom of the segment ($\Delta[CO_2^*]$), air flow rate f_{air} through the cuvette, [CO_2] of the air entering and exiting the cuvette ($\Delta[CO_2]$), length L of the stem segment and [CO_2^*] at start and end over a time period T ($\Delta[CO_2^*]_T$). The

second approach involves measurement of CO_2 and O_2 exchanges at the stem surface (Angert *et al.* 2012). Hereby, an indication of F_T can be obtained by calculating the apparent respiratory quotient (ARQ), which is defined as the ratio of CO_2 efflux to the atmosphere and O_2 influx into the stem. Carbohydrates are assumed as substrate for respiration. When no CO_2 is transported through the xylem (F_T = 0), CO_2 production and O_2 consumption should be equal, and the resulting ARQ will approximate one. If CO_2 is transported through the xylem, ARQ will deviate from one. In both approaches, the CO_2 fluxes are either calculated from measurements (mass balance approach) or indirectly estimated via a proxy (ARQ) (e.g. Teskey & Mcguire 2007; Salomón *et al.* 2018, 2019b; Hilman *et al.* 2019; Wang *et al.* 2019). Results capture net fluxes of internally transported CO_2 while specific dynamics are described with a low spatial resolution.

We propose a novel approach to quantify the fate of CO_2 dissolved in xylem sap ($CO_{2,X}$) based on radioactive $^{11}CO_2$ labelling coupled with positron emission tomography (PET). To this end, an aqueous solution of $^{11}CO_2$ was administered to the cut-end of branches of European aspen (*Populus tremula* L.). PET allowed *in vivo* visualisation of the dynamics of internally transported carbon with a high temporal resolution (every 2.5 min), resulting in 3D images with a high spatial resolution (± 1 mm). Image analysis resulted in direct estimates of the transport speed of xylem-transported CO_2 (v_{CO_2}). By means of compartmental modelling, v_{CO_2} estimation was refined, while also the relative contribution of $CO_{2,X}$ to the different carbon fluxes (Fig. 1) was determined. Revealing dynamics in $CO_{2,X}$ at high spatial and temporal resolution is essential to, for instance, better predict how plants cope with changing climate regimes. Furthermore, we believe that labelling of trees with radioactive isotopes is a promising technique to study plants *in vivo*.

Materials and methods

Plant material

For this study, 40-cm cuttings of *Populus tremula* L. (N = 3) were planted on March 23, 2016 in 30-L pots containing commercial potting mixture (Peltracom, Gent, Belgium). They were grown in a greenhouse for two months at the Faculty of Bioscience Engineering, Ghent University, Belgium (51.053693°N, 3.706487°E) and eventually had a height ranging between 90 and 120 cm. The trees were subsequently transported to the small animal imaging facility of Ghent University (INFINITY lab) 24 h before measurement (Pickard *et al.* 1993) where they were placed outdoors during the experiments. The cuttings were watered every day. The one-year-old study branches (N = 3, one branch per tree) had an average (±SE) length and diameter at their cut end of 21.17 ± 3.63 cm and 1.91 ± 0.10 mm, respectively.

Production and formulation of $^{11}CO_2$

The radioactive $^{11}CO_2$ was produced using a cyclotron (18 MeV protons, IBA, Belgium) of Ghent University Hospital a proton (i.e. H^+) was accelerated to a high velocity to bombard a N_2/H_2 (5%) target. The (p, α) nuclear reaction resulted in the formation of $^{11}CH_4$ which was subsequently oxidized via cobalt oxide to yield $^{11}CO_2$ as described by Landais & Finn (1989). Subsequently, $^{11}CO_2$ gas was bubbled through a 40 mM citric acid buffer at a set pH of *c.* 5.8, resembling the pH of xylem sap in young *P. tremula* branches (pH *c.* 6.4, which is in the reported range of 4.5 – 7.4 for woody species) (Teskey *et al.* 2008). The resulting ^{11}C-labelled solution was supplied to the cut end of the excised branches (one at a time). Once the solution is taken up by the branch, equilibrium reactions will shift according to the pH of the xylem sap (Butler 1991).

Experimental set-up and ^{11}C-labelling

Dynamics in internally transported CO_2 in the poplar branches was imaged following exposure to the ^{11}C-labelled solution. Radioactive labelling of the branches (one branch per day) was performed in an airtight chamber consisting of two compartments, a polypropylene labelling compartment (6 mL in volume) in which the cut end of the branch was exposed to the ^{11}C-label and a cylindrical plexiglass measurement compartment (135 mm inner diameter and 200 mm length) containing leaves and light source (ten red and blue LED lights, GreenPower LED strings 0842 LF Red and WPO 83 LF Blue, Philips, The Netherlands) providing about 250 µmol photons m^{-2} s^{-1} PAR to the leaves and branch (Fig. 2a). After cutting the branch under water, its position within the chamber was fixed by applying polysiloxane material (Terostat-IX, Henkel AG & Company, KGaA, Düsseldorf, Germany) around the branch at the intersection of both compartments to separate them. Extra grease (Vacuum grease, Dow Corning, Auburn, MI, USA) was added around the branch segment coming out of the polysiloxane material which ensured airtightness between both labelling and measurement compartments to avoid assimilation of evaporated $^{11}CO_2$ from the solution ($^{11}CO_2$ (aq) → $^{11}CO_2$ (g)) by leaf photosynthesis. To avoid leaf wilting the labelling compartment was filled with five mL of non-labelled buffer solution prior to the arrival of the label. A 5-mL volume was sufficient given the averaged transpiration rate (± SE) of 0.40 ± 0.01 mL h^{-1}. Because of the isotope's rapid decay, the labelling system was designed to give a minimal time-delay for the tracer to enter the branch after labelling. Therefore, the labelling compartment was connected to two 5-mL syringes (Fig. 2b). The first syringe, containing the ^{11}C-labeled solution, provided the tracer to the cut end of the branch. Just before introducing the tracer (orange arrow), the plunger of the second syringe was pulled to remove the non-labelled aqueous solution (yellow arrow). Five mL of $^{11}CO_2$-enriched solution was supplied to the branch with an activity at labelling of 125.8, 340.4 and 358.9 MBq, respectively, for

each of the experiments. A needle introduced at the headspace of the labelling compartment ensured in- and outflow of air (represented by the two-headed arrow having a yellow and orange colour, respectively) under these procedures so that no vacuum was created in the compartment. For safety measures, the outflowing air was directed to a container filled with soda lime to strip the $^{11}CO_2$ from the air. The branches were labelled for one hour.

The microclimate inside the measuring compartment was characterised by an average (± SE) relative humidity (RH), air temperature and vapor pressure deficit of 62.8 ± 2.3 %, 32.2 ± 1.3 °C and 1.80 ± 0.13 kPa, respectively. During the experiment air containing 400 ppm CO_2 was continuously supplied using a portable photosynthesis system (model LI-6400, Li-Cor Inc., Lincoln, NE, USA) as indicated by the green arrows in Fig. 2b. The H_2O and CO_2 content of the air coming in and out of the measuring compartment was analysed with a gas analyser (model LI-7000, Li-Cor Inc., Lincoln, NE, USA). To prevent radioactivity from coming into the atmosphere, the outflowing air was directed to a 1 M sodium hydroxide solution. Transpiration rate and photosynthetic rate, averaged (± SE) over the labelling periods, were 0.69 ± 0.14 mmol H_2O m^{-2} s^{-1} and 1.18 ± 0.38 µmol CO_2 m^{-2} s^{-1}, respectively.

PET scanner, image reconstruction and analysis

PET imaging was realised by application of a LabPET8 scanner (TriFoil Imaging, Chatsworth, CA, USA) which was located at the INFINITY imaging lab of Ghent University, Ghent, Belgium. The PET scanner is characterised by a relatively small ring of detectors (inner diameter and a depth of 15 and 7.5 cm, respectively) which defines the field of view (FOV). Hence, only a section of the measurement compartment that was inside the PET scanner was imaged. Normalisation and calibration of the PET detectors is done twice a year. For radiation safety purposes, the labelling compartment was shielded using lead sheets. After exposing the cut end of the study branch to the aqueous solution containing dissolved

$^{11}CO_2$ the PET scan was started and registered activity for one hour. PET images were eventually obtained via iterative reconstruction using the LabPET software (Version 1.12.1, TriFoil Imaging, Chatsworth, CA, USA). The maximum likelihood expectation maximization (MLEM) reconstruction algorithm was used to obtain an image showing ^{11}C-distribution within the FOV. Both a static 3D (i.e. x,y,z) and a dynamic 4D (i.e. x,y,z,t) reconstruction were performed per experiment using a 3D- or a 2D-MLEM algorithm, respectively. The 3D-MLEM algorithm allows coincidence counts (i.e. detection of gamma-photons originating from positron annihilation) between any of the detector rings whereas in the 2D-MLEM algorithm coincidences are counted only within a few consecutive rings of detectors (e.g. two or three rings) (Saha 2016). The 3D-MLEM reconstructed image therefore has a higher resolution compared to the 2D-MLEM reconstructed image and was used during image analysis for drawing regions of interest (ROIs - see further). On the contrary, 2D-MLEM reconstruction resulted in a quantitative image (voxels in MBq/ml) which could not be obtained using the 3D-MLEM algorithm of the LabPET software. 2D-MLEM reconstruction of the data allowed mutual comparison of experiments and was therefore applied to retrieve dynamic 4D ^{11}C-images. For both MLEM reconstruction algorithms 50 iterations were used, whereas the dynamic data was reconstructed into timeframes of 2.5 min. Correction for radioactive decay is performed during reconstruction so that a decay-corrected 3D and 4D image were obtained consisting of one (static) and 24 (dynamic) timeframe(s) with 63 slices of 200 × 200 voxels. Each voxel had a bit depth of 16 bits and a size of 0.5 × 0.5 × 1.175 mm. These images were imported in the open-source software tool AMIDE (Loening & Gambhir 2003) for image visualisation and analyses. Noise on the static image (Fig. 3 – upper left corner) was reduced using a 3D median filter with a kernel size of 3. On the resulting images, cylinder-shaped region of interests (ROIs) were drawn around the branch tissues along the direction of xylem flow. Up to six consecutive ROIs (input ROI, ROI 1-5,

Fig. 3 – upper left corner) were constructed, each having a length and diameter of 4 and 5 mm, respectively. Subsequently the dynamically reconstructed image was imported into the same file and the cumulative amount of ^{11}C-tracer in each ROI was calculated per 2.5 min timeframe (in MBq). Since the reconstructed images are corrected for decay, so are the resulting time-activity curves (TACs). The TACs (Fig. 4) were exported to be used as input for the compartmental model. An example of a dynamically reconstructed image is provided in Fig. 3 with 10 min temporal resolution.

The two dash dotted ROIs in the utmost proximal part of the branch (upper left corner of Fig. 3) were not used because a petiole was present on the branch segment enclosed in these ROIs. Due to the spatial resolution of the PET scanner (*c.* 1 mm) the petiole and branch could not be resolved on the reconstructed image and the ^{11}C-tracer detected in both branch and petiole was therefore added in these dotted ROIs. This caused an incorrectly higher tracer concentration (i.e. TACs – data not shown) with respect to the distally located ROIs. These TACs were therefore omitted for modelling because they would inevitably prompt wrong results upon parameter calibration. Hence, branch segments were selected without ramifications.

A first image-based estimation of the CO_2 transport speed through xylem ($v^*_{CO_2}$) was derived from the distance of an ROI from the cut end of the branch and the time at which the tracer was first detected in that ROI. However, given a temporal resolution of 2.5 min of the dynamic PET images, CO_2 transport speed could not be accurately determined. Hence, this parameter was seen as an initial value and included in the model calibration to be further refined. Student t-test was performed to denote statistical differences between the image-estimated and model-estimated CO_2 transport speed on a 5 % significance level ($p < 0.05$).

Compartmental modelling to compute characteristics of xylem-transported CO_2

The goal of fitting a compartmental model to dynamic tracer data through calibration was to derive specific parameters of xylem-transported CO_2 that have a physiological meaning and cannot be easily obtained from direct measurements. Due to the spatial resolution of the used PET scanner (*c.* 1 mm) physiological processes like the carbon fluxes between xylem and phloem tissues are integrated into the measured TACs (circles in Fig. 4) and therefore compartmental modelling is used to disentangle them. A compartmental model based on Bühler *et al.* (2011) and Hubeau *et al.* (2018) was implemented in the plant modelling software PhytoSim (Phyto-IT, Gent, Belgium) and fed with the TACs derived from ROIs from the image analysis (Fig. 5). Therefore, each ROI was divided into three compartments (Fig. 5), which correspond to the compartments defined in Fig. 1. The tracer concentration (T_C in MBq) of each compartment is described by Eqs. (2-4) where superscript denotes compartment number and subscript *i* the ROI number. Compartment 1 embodies xylem conduits and is characterized by the speed of xylem-transported CO_2 v_{CO_2} (mm min^{-1}) and the exchange constant *a* (min^{-1}), which represents the ratio of CO_2 that moves from xylem conduits into compartment 2 per minute, representing the surrounding xylem and phloem parenchyma and apoplastic spaces ($CO_{2,PA}$ in Fig. 1). From compartment 2, the ^{11}C-tracer is either directed towards chloroplast-containing cells where it is assimilated by P_{wt} (Fig. 1) and relocated in storage cells (compartment 3 in Fig. 5) via *b*, or radially diffused to the atmosphere via *c*. Chloroplast-containing tissues have been found in xylem ray cells (Rentzou & Psaras 2008) and pith tissue (van Cleve *et al.* 1993) but mainly in phloem and bark tissues (Pfanz & Aschan 2001; Saveyn *et al.* 2010). Exchange parameters *b* and *c* (both in min^{-1}) thus represent the net tracer fraction exchanged from compartment 2, which is assimilated via P_{wt} or alternatively diffuses to the atmosphere via efflux, respectively, and can be used to estimate the contribution of $CO_{2,X}$ to A_X and E_A of Eq. (1). Some CO_2 remains in

compartment 2 (i.e. xylem and phloem parenchyma and apoplastic spaces) to be temporarily stored as $CO_{2,PA}$ (ΔS of Eq. (1)). Note that the proposed model does not allow movement of $CO_{2,PA}$ in compartment 2 between different ROIs. This movement will therefore be incorporated in the estimation of v_{CO_2} but will be small compared to v_{CO_2} as xylem tissue is superior by means of transport properties. The parameter search range for v_{CO_2} was narrowed around the image-derived initial value $v^*_{CO_2}$ (which differed for each of the experiments). The search range for the other parameters was not adjusted.

$$\frac{dT_{C_i}^1}{dt} = \frac{v_{CO_2}}{l} \cdot T_{C_{i-1}}^1 - \frac{v_{CO_2}}{l} \cdot T_{C_i}^1 - a \cdot T_{C_i}^1 \quad (2)$$

$$\frac{dT_{C_i}^2}{dt} = a \cdot T_{C_i}^1 - b \cdot T_{C_i}^2 - c \cdot T_{C_i}^2 \quad (3)$$

$$\frac{dT_{C_i}^3}{dt} = b \cdot T_{C_i}^2 \quad (4)$$

Constant l is the length of the ROI (i.e. 4 mm). Parameters a, b and c represent fractions of xylem-transported CO_2 flowing across compartments and thus range from 0 to 1. Note that these parameters are the net result of ^{11}C-tracer flowing forth (e.g. a_{12}) and back (e.g. a_{21}) to each compartment because separate parameters (in- and outflow) were not identifiable. This approach is comparable with the fixed ratio (e.g. $a_{21} = h \times a_{12}$) implemented by Bühler *et al.* (2011). For the first timeframe, we assumed that all measured tracer was present in compartment 1. This assumption was tested, and it was found that the parameter outcome was insensitive to whether initial activity was allocated to compartment 1 only or distributed over all three compartments. Branch material was checked to ensure that the dimensions did not change with ROI since all model parameters were assumed to be constant for each ROI as well as over the entire scan time (i.e. 1 h). Note that this model allows CO_2 gas-liquid interconversion (Hari *et al.* 1991; Levy *et al.* 1999) but does not differentiate between phases.

Calibrated parameters should be taken with caution given that other carbon fluxes not accounted for by the model might bias parameter calibration.

The input ROI is most proximally located with respect to the other ROIs and does not receive tracer from any ROI. Because ^{11}C-tracer is actually transported into the input ROI, its total tracer amount (i.e. $T_{C_{total}}$) was used to calculate the tracer concentration in the first compartment for each time step according to Eq. (5). The change in tracer concentrations for the other two compartments was calculated according to Eqs. (3-4) with *i* = *input*.

$$T_{C}^{1}_{input} = T_{C_{total}} - T_{C}^{2}_{input} - T_{C}^{3}_{input} \quad (5)$$

Model sensitivity and identifiability analysis were evaluated according to De Pauw *et al.* (2008) by making use of the corresponding modules in the plant modelling software PhytoSim (Phyto-IT, Gent, Belgium). All four model parameters (v_{CO_2}, *a*, *b*, *c*) were found identifiable and were characterised by a high sensitivity for the model output. Parameter calibration was done by applying a shuffled complex evolution (Duan *et al.* 1993), with 9 complexes (i.e. two times number of model parameters + 1, which was found to result in a better overall calibration performance as described by Duan *et al.* (1994)) and an accuracy of 10^{-5}, for 5000 evaluations. Using the resulting model parameters, continuous data was simulated using an adaptive step size fourth order Runge-Kutta solver (accuracy 10^{-5}, maximum step size 1 min) (Runge 1895; Kutta 1901; De Pauw *et al.* 2008). Calibration was completed when the difference between simulated and measured TACs was minimized. Through the uncertainty analysis 95% confidence interval of the estimated model parameters were obtained.

Data processing and terminology

To assess the correlation between v_{CO_2} and the transpiration rate, the computed exchange parameters (*a*, *b* and *c*) and the carbon fluxes ($F_T^{\%}/CO_{2,X}$, $\Delta S^{\%}/CO_{2,X}$ and $E_A^{\%}/CO_{2,X}$), a standard major axis (SMA) regression model was fitted in RStudio (R Core Team (2018), RStudio: Integrated Development Environment for R. RStudio, Inc., Boston, MA, USA, version 1.1.463) using the *lmodel2* function, in which v_{CO_2} was treated as independent variable whereas transpiration rate, exchange parameters and carbon fluxes were treated as dependent variables. An SMA regression model was used instead of a linear model since v_{CO_2} (x-variable) is not fixed and has an error (i.e. SE). Normality of the variables was tested and found by Shapiro-Wilk test (on a 5% significance level), justifying the application of an SMA model. The SMA regression model resulted in p-values indicating whether or not the slope was significant at a 5 % significance level ($p < 0.05$) and a coefficient of determination (R^2). When the slope was significant, a significant increase or decrease was mentioned. When the slope was not significant a tendency towards a positive or negative correlation was indicated.

Assessing the fate of xylem-transported CO_2 using PET and compartmental modelling

Exchange parameters *a*, *b* and *c* describe the fate of the xylem-transported CO_2 with respect to net radial diffusion, assimilation A_X by P_{wt} and efflux to the atmosphere, respectively. These parameters can be used to estimate the relative contribution of xylem-dissolved CO_2 ($CO_{2,X}$) to each of the carbon fluxes ($F_T^{\%}/CO_{2,X}$, $\Delta S^{\%}/CO_{2,X}$ and $E_A^{\%}/CO_{2,X}$) in accordance with the model described by McGuire & Teskey 2004 (Eq. (1)). Additionally, our method allows to identify the relative amount of $CO_{2,X}$ that is assimilated through P_{wt} (i.e. $A_X^{\%}/CO_{2,X}$).

Specifically, parameter *a* indicates CO_2 exchange from the xylem conduits to the surrounding parenchyma and apoplastic spaces (i.e. $CO_{2,PA}$). Hence, fraction (1 – *a*) of the $^{11}CO_2$-tracer was transported upwards on a minute basis representing $F_T^{\%}/CO_{2,X}$. CO_2 that is present in the parenchyma and apoplastic spaces ($CO_{2,PA}$) can be assimilated through P_{wt} (via *b* to

compartment 3 of the model in Fig. 5) or be released to the atmosphere via efflux (via *c*). Hence, to estimate the corresponding xylem-transported CO_2 fractions multiplication of exchange parameters *b* and *c* with *a* was performed, as these products can be related to the relative CO_2 fluxes $A_X^{\%}/CO_{2,X}$ (i.e. assimilation flux) and $E_A^{\%}/CO_{2,X}$ (i.e. efflux to the atmosphere), respectively. The remaining $CO_{2,PA}$ $(1 - b - c)$ can be multiplied with *a* to retrieve the storage flux $\Delta S^{\%}$. The relative contribution of the each of the carbon fluxes is given in Eq. (6).

$$1 = (1 - a) + (a \times b) + (a \times c) + (a \times (1 - b - c)) \quad (6)$$
$$F_T^{\%}/CO_{2,X} \quad A_X^{\%}/CO_{2,X} \quad E_A^{\%}/CO_{2,X} \quad \Delta S^{\%}/CO_{2,X}$$

Results

PET images

Tracer transport from the proximal (left) part of the branch to the distal part is shown in Fig. 3. Highest tracer concentration was observed in the proximal part. The normalised sum of tracer concentrations (± SE) over the scanning period of one hour per ROI (averaged over all three experiments) is given in Fig. 6. Tracer concentration per ROI was normalised with the input ROI concentration.

Modelling xylem-transported carbon dynamics

Time series of tracer concentration within each ROI (Fig. 4) showed that ^{11}C-tracer concentration increased with time. Each distally located ROI showed a lower concentration with respect to the adjacent proximal ROI (Fig. 6). This can be linked to the lower slope of the TACs for the distal ROIs compared to the proximal ROIs (Fig. 4) indicating local retention of tracer due to A_X and/or tracer efflux to the atmosphere.

Measured TACs were used for compartmental modelling and closely corresponded with the simulated TACs (Fig. 4). In the study branches (N = 3), average (± SE) model-estimated speed of xylem-transported CO_2 v_{CO_2} (for the compartmental model in Fig. 5) was found to be 5.00 ± 1.29 mm min^{-1} and was not significantly different ($p > 0.05$) from the average (± SE) image-estimated $v^*_{CO_2}$ (based on the distance of an ROI from the cut end of the branch and the time at which the tracer was first detected in that ROI), which equalled 5.55 ± 2.15 mm min^{-1} (Fig. 7a). The exchange rate parameters *a* (i.e. tracer fraction from xylem conduits to the surrounding xylem and phloem parenchyma and apoplastic spaces), *b* (i.e. the fraction of $CO_{2,PA}$ that gets assimilated by P_{wt}) and *c* (i.e. the tracer fraction that diffuses to the atmosphere via efflux) averaged (± SE) over the experimental branches (N = 3) 0.51 ± 0.06, 0.71 ± 0.07 and 0.25 ± 0.06 min^{-1} (Fig. 7b). Note that actual exchange fractions might be higher than the obtained model-estimates, because our parameters represent net exchange between tissues/compartments.

The average (± SE) relative contribution of the CO_2 fluxes $F_T^{\%}/CO_{2,X}$, $A_X^{\%}/CO_{2,X}$, $E_A^{\%}/CO_{2,X}$ and $\Delta S^{\%}/CO_{2,X}$ equaled 0.49 ± 0.06, 0.38 ± 0.08, 0.12 ± 0.01 and 0.01 ± 0.01 min^{-1}, respectively, and their sum equals one. Note that the fraction of CO_2 that remains inside the parenchyma and apoplastic spaces ($\Delta S^{\%}/CO_{2,X}$) is neglectable.

Tendency towards a positive correlation was found between the transpiration rate and the transport speed of xylem-transported CO_2, i.e. v_{CO_2} (Fig. 8a). Tendency towards a positive correlation was obtained for the exchange parameters *a*, *b* and v_{CO_2} (p-value 0.15 and 0.22, respectively - Fig. 8b) and $A_X^{\%}/CO_{2,X}$ and v_{CO_2} (p-value 0.16 - Fig. 8c). A tendency to an inverse correlation was found between parameter *c* and v_{CO_2} (p-value 0.23 - Fig. 8b) and between carbon fluxes $F_T^{\%}/CO_{2,X}$, $E_A^{\%}/CO_{2,X}$ and $\Delta S^{\%}/CO_{2,X}$ and v_{CO_2} (p-value 0.15, 0.27 and 0.05, respectively - Fig. 8c).

Discussion

Plant–PET to unravel dynamics in woody tissue photosynthesis

Preceding to compartmental modelling, pure image analysis demonstrated that highest ^{11}C-concentrations were found in the proximal branch parts (Figs. 4 and 6). Part of the ^{11}C-tracer hence accumulated during the scanning period, indicating assimilation of CO_2 by P_{wt}. Comparable results were obtained in detached sycamore branches that were allowed to take up $^{13}CO_2$-labelled solution (McGuire *et al.* 2009). Moreover, highest ^{13}C-enrichment was found in the lower branch sections due to their proximity to the ^{13}C-source. Regarding the transport speed of CO_2, a first image-estimated $v^*_{CO_2}$ was obtained by determining which specific branch segment was inside the FOV of the PET scanner. This is, to our understanding, a first method to directly determine the speed of xylem-transported CO_2 *in vivo*. Given the temporal resolution of 2.5 min of the dynamic PET images, this initial value was subsequently used to narrow the search range of model-estimated v_{CO_2} upon parameter calibration.

The compartmental model was able to simulate the behaviour of internally transported CO_2 in young branches, resulting in a close correspondence between measured and simulated time–tracer curves of ^{11}C-tracer (Fig. 4). No significant difference ($p > 0.05$) was found between $v^*_{CO_2}$ and v_{CO_2}, indicating the validity of the proposed measurement techniques, i.e. direct image- and model- estimation of CO_2 transport speed. Since CO_2 is transported through the xylem, v_{CO_2} is expected to be linked to the sap flow rate (McGuire & Teskey 2004; Bloemen *et al.* 2013c; Salomón *et al.* 2018). This rationale is also used in the mass balance approach (Eq. 1; McGuire & Teskey 2004) as sap flow is used to calculate the carbon flux through the xylem. This explains the tendency towards a positive correlation between the transpiration rate and v_{CO_2} (Fig. 8a).

Aside from the CO_2 transport speed v_{CO_2}, other dynamic characteristics of xylem-transported CO_2 within *P. tremula* branches were assessed using a combination of PET scans and compartmental modelling. Model calibration successfully resulted in the exchange parameters *a*, *b* and *c* describing the relative carbon transport fluxes originating from $CO_{2,X}$. Analogous to the mass balance approach described by McGuire & Teskey (2004), we propose dynamic ^{11}C-PET combined with compartmental modelling yielding the exchange parameters as a new method to further disentangle the different carbon fluxes inside woody tissues. Our method results in the relative contribution of $CO_{2,X}$ to each of the carbon fluxes of the mass balance ($F_T^{\%}/CO_{2,X}$, $\Delta S^{\%}/CO_{2,X}$ and $E_A^{\%}/CO_{2,X}$) as well as $A_X^{\%}/CO_{2,X}$ of which the sum equals one. When measuring [CO_2^*] (µmol CO_2 L^{-1}) inside branches and branch water content (L m^{-3}), it is possible to quantify each of the relative carbon fractions in Eq. (6) to fluxes expressed in µmol CO_2 m^{-3} min^{-1}. However, note that the obtained relative carbon fluxes are not comparable with the carbon fluxes of the mass balance described by McGuire & Teskey (2004) because our study only focusses on the fate of xylem-transported CO_2 ($CO_{2,X}$). Hence, the sum of the relative fluxes does not represent stem respiration R_S. Comparison with the mass balance fluxes boils down to determining the part of R_S dissolving in the sap at small spatial scale. Comparison with studies involving xylem sap labelling is of course justified.

In young branches of *P. tremula*, it was found that slightly less than half (0.49 min^{-1}) of the $^{11}CO_2$-tracer was transported upwards on a minute basis representing the contribution of $F_T^{\%}/CO_{2,X}$. This is plausible as a study where 7-yr-old field-grown poplar trees were infused with $^{13}CO_2$-labeled solution into the base for two days described ^{13}C-enrichment throughout the entire tree (stem, branch woody tissues and foliage) suggesting substantial tracer movement (Bloemen *et al.* 2013b). The same trend was observed for a similar study on 4-m tall northern white-cedar trees (Powers & Marshall 2011). Additionally, a study where

detached 20-50 cm long branches (<1 cm in diameter) of a 7-year-old *P. deltoides* tree were labelled with aqueous $^{13}CO_2$-enriched solutions (having different label concentration) found that at least 29% of the assimilated ^{13}C-label was fixed in the branches (with the remaining part in leaves) (Bloemen *et al.* 2013a). These results suggest that most of the label was transported to the leaves to be assimilated. They can however not be used to predict $F_T^{\%}/CO_{2,X}$, which is an advantage of ^{11}C-based PET over ^{13}C-based labelling.

Relative xylem-transported CO_2-fraction contributing to the assimilation flux $A_X^{\%}/CO_{2,X}$ (0.38) lies within the assimilation percentage (35 – 42 %) of young branches of poplar and sycamore that could take up a $^{13}CO_2$-labelled solution (McGuire *et al.* 2009; Bloemen *et al.* 2013c). However, it is rather low compared to the reported reassimilation percentage of woody species (40 – 123%) (Teskey *et al.* 2008; Ávila *et al.* 2014). Reassimilation higher than 100% are associated with net CO_2 uptake via lenticels in the stem periderm (Berveiller *et al.* 2007) but was not taken into account in this study. Furthermore, parameter *b* indicates that most of the available $CO_{2,PA}$ was assimilated instead of directed to the atmosphere (0.71 vs. 0.25 - Fig. 7b). This is in accordance to the high A_X efficiency of P_{wt} observed in young *P. tremula* branches and petioles which are characterised by thin and smooth bark having a high content of chloroplasts (Aschan *et al.* 2001; Ávila *et al.* 2014; De Roo *et al.* 2019). However, upon development of the periderm, a reduction in light transmittance can be expected, causing a reduction in A_X efficiency of P_{wt} (Ávila *et al.* 2014).

The relative fraction of xylem-transported CO_2 that was direct to the atmosphere via efflux $E_A^{\%}/CO_{2,X}$ was limited (0.12) and is related to the high assimilation of CO_2 by P_{wt}. Specifically, A_X in the light has been estimated to reduce CO_2 efflux from branches by about 52% (McGuire *et al.* 2009). Hence, it is expected that CO_2 efflux would increase when the branches would not have been irradiated with PAR.

Dependency of internal CO_2 fluxes on transport speed

Since sap flow and thus the transport speed of CO_2 is found to substantially affect both the efficiency of P_{wt} and the efflux to the atmosphere (Teskey & McGuire 2002; McGuire *et al.* 2007; Teskey *et al.* 2008; Bloemen *et al.* 2013c; Ávila *et al.* 2014; Stutz & Hanson 2019) the exchange parameter values of each experiment are described as function of v_{CO_2}. Exchange parameter *a* had a tendency to increase with increasing v_{CO_2} (Fig. 8b) which might be explained by the fact that more CO_2 is delivered to the tissue at a higher transport speed. Studies in which the mass balance approach of McGuire & Teskey (2004) has been applied suggest an increasing $F_T^{\%}/CO_{2,X}$ (calculated as 1 – *a* in this study) with increasing v_{CO2} since higher F_T-values are obtained during the day (i.e. when transpiration and thus internal CO_2 transport is higher) than during the night (McGuire & Teskey 2004; Salomón *et al.* 2018). On the contrary, in our study, a decrease in $F_T^{\%}/CO_{2,X}$ is observed with increasing v_{CO2} which can be linked to the increasing assimilation $A_X^{\%}/CO_{2,X}$ with increasing v_{CO_2} (Fig. 8c). The reason for this discrepancy is related to the exclusion of woody tissue photosynthesis and thus A_X in mass balance studies due to the application of opaque cuvettes making these results incomparable. The observed decrease in $F_T^{\%}/CO_{2,X}$ with increasing v_{CO_2} in our study is valid given its similarity to the inverse relation found between xylem sap flux density and [CO_2^*] in the stem of a *Liriodendron tulipifera* tree (Teskey & McGuire 2002). Similarly, increasing sap flux density resulted in a rapid decrease in xylem [CO_2^*] in *Platanus occidentalis* branches (McGuire *et al.* 2007).

Since assimilation of xylem-transported CO_2 is dependent on transpiration rate (Bloemen *et al.* 2013c; Mincke *et al.* 2018), which provides substrate for photosynthetic reactions, a tendency to a positive correlation was found between *b* and v_{CO_2} (Fig. 8b), and hence between assimilation flux $A_X^{\%}/CO_{2,X}$ and v_{CO_2} (Fig. 8c). The observed trend is in accordance to a study were leaf transpiration rates in detached poplar branches were altered,

while branches were allowed to take up $^{13}CO_2$ solution (Bloemen *et al.* 2013c). Through stable isotope ^{13}C-analysis of branch tissues it was found that woody tissues assimilated more ^{13}C-label under higher transpiration. As $A_X^{\%}/CO_{2,X}$ increases with increasing v_{CO_2} (Fig. 8c), it might be theorized that Rubisco present in the chlorophyll-containing woody tissues is not saturated with CO_2 under the experimental conditions. Photosynthetic contribution of $CO_{2,X}$ to the carbon budget should therefore not be neglected in (green) woody tissues.

Both the CO_2 to be assimilated via P_{wt} (via *b*) or directed to the atmosphere via efflux (via *c*) originated from CO_2 present in parenchyma and apoplastic spaces ($CO_{2,PA}$). Hence, an increasing parameter *b* with rising v_{CO2} (Fig. 8b) results in a decreasing parameter *c*. However, radial diffusion $E_A^{\%}/CO_{2,X}$ remains constant for varying v_{CO2} values (Fig. 8c), which can be related to the inverse effect of v_{CO2} on the model parameters *a* and *c,* and hence the neutralizing effect on $E_A^{\%}/CO_{2,X}$, which is calculated from *a* and *c*. Additionally, since parameter *c* has a non-zero value, our results indicate that part of xylem-transported $^{11}CO_2$ radially diffused to the atmosphere which illustrates the error incurred when R_S is estimated from E_A measurements (McGuire & Teskey 2004; Teskey *et al.* 2008; Trumbore *et al.* 2013). By means of isotopic labelling coupled with isotope ratio laser spectroscopy, Salomón *et al.* (2019) disentangled the contribution of locally respired CO_2 (L_{CO2}) and xylem transported CO_2 (T_{CO2}) to E_A for *P. tremula*. When the contribution of both T_{CO2} and L_{CO2} to E_A is desired, the current experimental set-up requires measurements of E_A and internal sap [CO_2^*].

Conclusion

Tracing xylem-transported $^{11}CO_2$ in young *P. tremula* branches using the medical imaging technique positron emission tomography (PET) enabled visualising its dynamics *in vivo* with high spatial and temporal resolution. We demonstrated the applicability of dynamic PET imaging in combination with compartmental modelling to quantify the transport speed of

internal CO_2 (v_{CO2}) as well as to retrieve dynamics in xylem-transported CO_2 with regard to upward transport with the sap (F_T), assimilation via P_{wt} (A_X) and efflux to the atmosphere (E_A). P_{wt} may efficiently reduce respiratory CO_2 losses, at least in young twigs and branches, and thus in the outer parts of tree crowns. Hence, refixation of CO_2 appears to be of great importance for carbon budgets in e.g. environmentally controlled leafless states of deciduous trees (although surely different in young and mature trees). Increasing the number of replications, including both smaller and larger sized branches, is needed to further confirm our results and could result in a statistically significant regression of the model parameters in function of v_{CO2}.

Nonetheless, our findings indicate the potential of plant-PET since physiological parameters are obtained regarding the fate of internally transported CO_2 that are otherwise challenging to be measured with the same spatial resolution. Therefore, we believe that *in vivo* imaging in combination with modelling, both at cell and organ scale, are necessary to advance our mechanistic understanding of plant physiology, including P_{wt}.

Conflict of Interest Statement

Non declared.

Funding

This project was supported by a starting grant from the Scientific Research Foundation Flanders (FWO) by research program G.0319.13N to KS and SV; and SB fellowship 1S37716N granted to JM.

Acknowledgements

The authors wish to thank Philip Deman and Geert Favyts of the Laboratory of Plant Ecology, Ghent University, for their enthusiastic technical and practical support, and Benedict Descamps of the INFINITY lab, Ghent University, for the technical help and tips during the PET experiments. Sincere gratitude goes to Dr. Roberto Salomón for his important remarks and suggestions.

Authors' contribution

JM and KS designed the research. JC produced and administered the radioactivity. JM performed the experiments. JM and KS analysed and interpreted the data. JM wrote the first draft of the manuscript. All authors read and edited the manuscript before publication under supervision of KS.

References

Amthor, J.S. (2000). The McCree-de Wit-Penning de Vries-Thornley respiration paradigms: 30 Years later. *Ann. Bot.*, 86, 1–20.

Angert, A., Muhr, J., Negron Juarez, R., Alegria Muñoz, W., Kraemer, G., Ramirez Santillan, J., *et al.* (2012). Internal respiration of Amazon tree stems greatly exceeds external CO_2 efflux. *Biogeosciences*, 9, 4979–4991.

Aschan, G., Wittmann, C. & Pfanz, H. (2001). Age-dependent bark photosynthesis of aspen twigs. *Trees - Struct. Funct.*, 15, 431–437.

Atkin, O.K. & Macherel, D. (2009). The crucial role of plant mitochondria in orchestrating drought tolerance. *Ann. Bot.*, 103, 581–597.

Aubrey, D.P. & Teskey, R.O. (2009). Root-derived CO_2 efflux via xylem stream rivals soil CO_2 efflux. *New Phytol.*, 184, 35–40.

Ávila, E., Herrera, A. & Tezara, W. (2014). Contribution of stem CO_2 fixation to whole-plant carbon balance in nonsucculent species. *Photosynthetica*, 52, 3–15.

Berveiller, D., Kierzkowski, D. & Damesin, C. (2007). Interspecific variability of stem photosynthesis among tree species. *Tree Physiol.*, 27, 53–61.

Bloemen, J., Mcguire, M.A., Aubrey, D.P., Teskey, R.O. & Steppe, K. (2013a). Internal recycling of respired CO_2 may be important for plant functioning under changing climate regimes. *Plant Signal. Behav.*, 8.

Bloemen, J., Mcguire, M.A., Aubrey, D.P., Teskey, R.O. & Steppe, K. (2013b). Transport of root-respired CO_2 via the transpiration stream affects aboveground carbon assimilation and CO_2 efflux in trees. *New Phytol.*, 197, 555–565.

Bloemen, J., McGuire, M.A., Aubrey, D.P., Teskey, R.O. & Steppe, K. (2013c). Assimilation of xylem-transported CO_2 is dependent on transpiration rate but is small relative to atmospheric fixation. *J. Exp. Bot.*, 64, 2129–2138.

Bloemen, J., Vergeynst, L.L., Overlaet-Michiels, L. & Steppe, K. (2016). How important is woody tissue photosynthesis in poplar during drought stress? *Trees - Struct. Funct.*, 30, 63–72.

Bühler, J., Huber, G., Schmid, F. & Blümler, P. (2011). Analytical model for long-distance tracer-transport in plants. *J. Theor. Biol.*, 270, 70–79.

Butler, J.N. (1991). *Carbon Dioxide Equilibria and their Applications*. 1st editio. CRC Press, New York, NY.

Cernusak, L.A. & Cheesman, A.W. (2015). The benefits of recycling: How photosynthetic bark can increase drought tolerance. *New Phytol.*, 208, 995–997.

Cernusak, L.A. & Marshall, J.D. (2000). Photosynthetic rexation in branches of Western White Pine. *Funct. Ecol.*, 14, 300–311.

van Cleve, B., Forreiter, C., Sauter, J.J. & Apel, K. (1993). Pith cells of poplar contain photosynthetically active chloroplasts. *Planta*, 189, 70–73.

Duan, Q., Sorooshian, S. & Gupta, V.K. (1994). Optimal use of the SCE-UA global optimization method for calibrating watershed models. *J. Hydrol.*, 158, 265–284.

Duan, Q.Y., Gupta, V.K. & Sorooshian, S. (1993). Shuffled complex evolution approach for effective and efficient global minimization. *J. Optim. Theory Appl.*, 76, 501–521.

Hari, P., Nygren, P. & Korpilahti, E. (1991). Internal circulation of carbon within a tree. *Can. J. For. Res.*, 21, 514.

Hilman, B., Muhr, J., Trumbore, S.E., Kunert, N., Carbone, M.S., Yuval, P., *et al.* (2019). Comparison of CO_2 and O_2 fluxes demonstrate retention of respired CO_2 in tree stems from a range of tree species. *Biogeosciences*, 16, 177–191.

Höltta, T. & Kolari, P. (2009). Interpretation of stem CO_2 efflux measurements. *Tree Physiol.*, 29, 1447–1456.

Hubeau, M., Mincke, J., Vanhove, C., Courtyn, J., Vandenberghe, S. & Steppe, K. (2018).

Plant-PET to investigate phloem vulnerability to drought in *Populus tremula* under changing climate regimes. *Tree Physiol.*, 39, 211–221.

Kutta, W. (1901). Beitrag zur näherungweisen Integration totaler Differentialgleichungen. *Math. Phys.*, 46, 435–453.

Landais, P. & Finn, R. (1989). On-line preparation of [^{11}C]carbon dioxide from [^{11}C]methane. *Int. J. Radiat. Appl. Instrumentation. Part A. Appl. Radiat. Isot.*, 40, 265–266.

Levy, P.E., Meir, P., Allen, S.J. & Jarvis, P.G. (1999). The effect of aqueous transport of CO_2 in xylem sap on gas exchange in woody plants. *Tree Physiol.*, 19, 53–58.

Loening, A.M. & Gambhir, S.S. (2003). AMIDE: A Free Software Tool for Multimodality Medical Image Analysis. *Mol. Imaging*, 2, 131–137.

McGuire, M.A., Cerasoli, S. & Teskey, R.O. (2007). CO_2 fluxes and respiration of branch segments of sycamore (*Platanus occidentalis* L.) examined at different sap velocities, branch diameters, and temperatures. *J. Exp. Bot.*, 58, 2159–2168.

McGuire, M.A., Marshall, J.D. & Teskey, R.O. (2009). Assimilation of xylem-transported ^{13}C-labelled CO_2 in leaves and branches of sycamore (*Platanus occidentali*s L.). *J. Exp. Bot.*, 60, 3809–3817.

McGuire, M.A. & Teskey, R.O. (2004). Estimating stem respiration in trees by a mass balance approach that accounts for internal and external fluxes of CO_2. *Tree Physiol.*, 24, 571–578.

Mincke, J., Hubeau, M., Cortyn, J., Brans, B., Vanhove, C., Vandenberghe, S., *et al.* (2018). Normalization of ^{11}C-autoradiographic images for semi-quantitative analysis of woody tissue photosynthesis . *Acta Hortic.*, 35–42.

De Pauw, D.J.W., Steppe, K. & De Baets, B. (2008). Identifiability analysis and improvement of a tree water flow and storage model. *Math. Biosci.*, 211, 314–332.

Pfanz, H. (2008). Bark photosynthesis. *Trees - Struct. Funct.*, 22, 137–138.

Pfanz, H. & Aschan, G. (2001). The Existence of Bark and Stem Photosynthesis in Woody Plants and Its Significance for the Overall Carbon Gain. An Eco-Physiological and Ecological Approach. In: *Progress in Botany* (eds. Esser, K., Lüttge, U., Kadereit, J.W. & Beyschlag, W.). Springer Berlin Heidelberg, Berlin, pp. 477–510.

Pickard, W.F., Minchin, P.E.H. & Thorpe, M.R. (1993). Leaf export and partitioning changes induced by short-term inhibition of phloem transport. *J. Exp. Bot.*, 44, 1491–1496.

Powers, E.M. & Marshall, J.D. (2011). Pulse labeling of dissolved ^{13}C-carbonate into tree xylem: Developing a new method to determine the fate of recently fixed photosynthate. *Rapid Commun. Mass Spectrom.*, 25, 33–40.

R Core Team. (2018). *R: A language and environment for statistical computing*. Available at: https://www.r-project.org/. Last accessed .

Rentzou, A. & Psaras, G.K. (2008). Green plastids, maximal PSII photochemical efficiency and starch content of inner stem tissues of three Mediterranean woody species during the year. *Flora Morphol. Distrib. Funct. Ecol. Plants*, 203, 350–357.

De Roo, L., Bloemen, J., Dupon, Y., Salomón, R.L. & Steppe, K. (2019). Axial diffusion of respired CO_2 confounds stem respiration estimates during the dormant season. *Ann. For. Sci.*, 76.

Runge, C. (1895). Über die numerische Auflösung von Differentialgleichungen. *Math. Ann.*, 46, 167–178.

Saha, G.B. (2016). *Basics of PET imaging: Physics, chemistry, and regulations, third edition. Basics PET Imaging Physics, Chem. Regul. Third Ed.*

Salomón, R.L., De Roo, L., Bodé, S., Boeckx, P. & Steppe, K. (2019a). Isotope ratio laser spectroscopy to disentangle xylem-transported from locally respired CO_2 in stem CO_2 efflux. *Tree Physiol.*, 39, 819–830.

Salomón, R.L., De Schepper, V., Valbuena-Carabaña, M., Gil, L. & Steppe, K. (2018). Daytime depression in temperature-normalised stem CO_2 efflux in young poplar trees is dominated by low turgor pressure rather than by internal transport of respired CO_2. *New Phytol.*, 217, 586–598.

Salomón, R.L., Steppe, K., Crous, K.Y., Noh, N.J. & Ellsworth, D.S. (2019b). Elevated CO_2 does not affect stem CO_2 efflux nor stem respiration in a dry Eucalyptus woodland, but it shifts the vertical gradient in xylem [CO_2]. *Plant Cell Environ.*, 42, 2151–2164.

Saveyn, A., Steppe, K., Ubierna, N. & Dawson, T.E. (2010). Woody tissue photosynthesis and its contribution to trunk growth and bud development in young plants. *Plant, Cell Environ.*, 33, 1949–1958.

Steppe, K., Saveyn, A., McGuire, M.A., Lemeur, R. & Teskey, R.O. (2007). Resistance to radial CO_2 diffusion contributes to between-tree variation in CO_2 efflux of *Populus deltoides* stems. *Funct. Plant Biol.*, 34, 785–792.

Steppe, K., Sterck, F. & Deslauriers, A. (2015). Diel growth dynamics in tree stems: Linking anatomy and ecophysiology. *Trends Plant Sci.*, 20, 335–343.

Stringer, J.W. & Kimmerer, T.W. (1993). Refixation of xylem sap CO_2 in *Populus deltoides*. *Physiol. Plant.*, 89, 243–251.

Stutz, S.S., Anderson, J., Zulick, R. & Hanson, D.T. (2017). Inside out: Efflux of carbon dioxide from leaves represents more than leaf metabolism. *J. Exp. Bot.*, 68, 2849–2857.

Stutz, S.S. & Hanson, D.T. (2019). Contribution and consequences of xylem-transported CO_2 assimilation for C_3 plants. *New Phytol.*, 223, 1230–1240.

Teskey, R., McGuire, M., Bloemen, J., Aubrey, D. & Steppe, K. (2017). Plant respiration: metabolic fluxes and carbon balance. In: *Respiration and CO_2 fluxes in trees* (eds. Tcherkez, G. & Ghashghaie, J.). Springer International Publishing, Cham, pp. 181–207.

Teskey, R., Teskey, R.O., Saveyn, A., Steppe, K. & Mcguire, M.A. (2008). Origin, fate and

significance of CO_2 in tree stems. *New Phytol.*, 177, 17–32.

Teskey, R.O. & Mcguire, M.A. (2007). Measurement of stem respiration of sycamore (*Platanus occidentalis* L.) trees involves internal and external fluxes of CO_2 and possible transport of CO_2 from roots. *Plant, Cell Environ.*, 30, 570–579.

Teskey, R.O. & McGuire, M.A. (2002). Carbon dioxide transport in xylem causes errors in estimation of rates of respiration in stems and branches of trees. *Plant, Cell Environ.*, 25, 1571–1577.

Thornley, J.H.M. (2011). Plant growth and respiration re-visited: Maintenance respiration defined it is an emergent property of, not a separate process within, the system and why the respiration: Photosynthesis ratio is conservative. *Ann. Bot.*, 108, 1365–1380.

Trumbore, S.E., Angert, A., Kunert, N., Muhr, J. & Chambers, J.Q. (2013). What's the flux? Unraveling how CO_2 fluxes from trees reflect underlying physiological processes. *New Phytol.*, 197, 353–355.

Vandegehuchte, M.W., Bloemen, J., Vergeynst, L.L. & Steppe, K. (2015). Woody tissue photosynthesis in trees: Salve on the wounds of drought? *New Phytol.*, 208, 998–1002.

Wang, X., Mao, Z., McGuire, M.A. & Teskey, R.O. (2019). Stem radial CO_2 conductance affects stem respiratory CO_2 fluxes in ash and birch trees. *J. For. Res.*, 30, 21–29.

Figure captions

Figure 1 Schematic illustrating the fate of respired CO_2 in woody tissues. Internal transport of xylem-transported CO_2 (F_T) can diffuse to the surrounding xylem and phloem parenchyma and apoplastic spaces (represented by $CO_{2,PA}$) from where it can either radially diffuse into the atmosphere via stem CO_2 efflux (E_A) or be assimilated (A_X) by chloroplasts present in the bark, and xylem rays, which is known as woody tissue photosynthesis (P_{wt}). The remaining part is stored (ΔS) as $CO_{2,PA}$. Xylem and outer tissues (cambium, phloem and bark) are represented in dark and light brown, respectively. The cylinder enclosing the stem segment represents one ROI of the model described in Fig. 5. Arrows indicate model parameters with v_{CO_2} the transport speed of CO_2 (mm min^{-1}) while *a*, *b* and *c* represent CO_2 exchange fractions (min^{-1}).

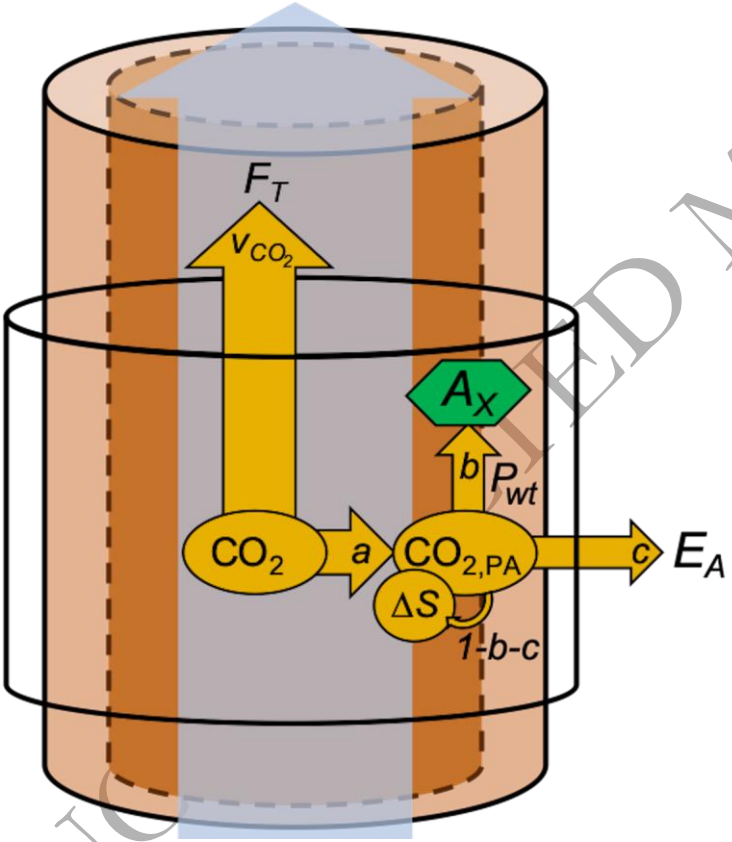

Figure 2 Schematic of the experimental set-up displaying a *P. tremula* branch inside an airtight chamber (a) and syringe set-up to provide ^{11}C-label (b). A small and dark cylindrical labelling compartment with an aqueous solution containing $^{11}CO_2$ (indicated in orange) and the cut end of the branch is hermetically sealed from the measurement compartment containing the illuminated part of the branch. The measurement compartment was positioned in the circular bore of the PET scanner and only a part of it was surrounded by the detector ring (i.e. the FOV of the PET scanner). The incoming [CO_2] is maintained at 400 ppm by a LI-6400 system while the water content and [CO_2] entering and leaving the measurement compartment is analysed by a LI-7000 system, to calculate the transpiration and photosynthetic rate, respectively. Measurement of the flow rate of the air entering and leaving the measurement compartment enabled detection of undesired leaks. For safety measures, the leaving air is stripped from all radioactivity by bubbling it through a basic NaOH solution. Regarding the introduction of ^{11}C-tracer (b) the labelling compartment was connected to two 5-mL syringes. The first syringe, containing the ^{11}C-tracer solution, provided the tracer to the cut end of the branch (orange arrow). Just before introducing the tracer, the plunger of the second syringe was pulled to remove the non-labelled aqueous solution (yellow arrow). A needle introduced at the headspace of the labelling compartment ensured in- and outflow of air (represented by the two-headed arrow having a yellow and orange colour, respectively) under these procedures so that no vacuum was created in the compartment. For safety measures, the outflowing air was directed to a container filled with soda lime as to strip the $^{11}CO_2$ from the air.

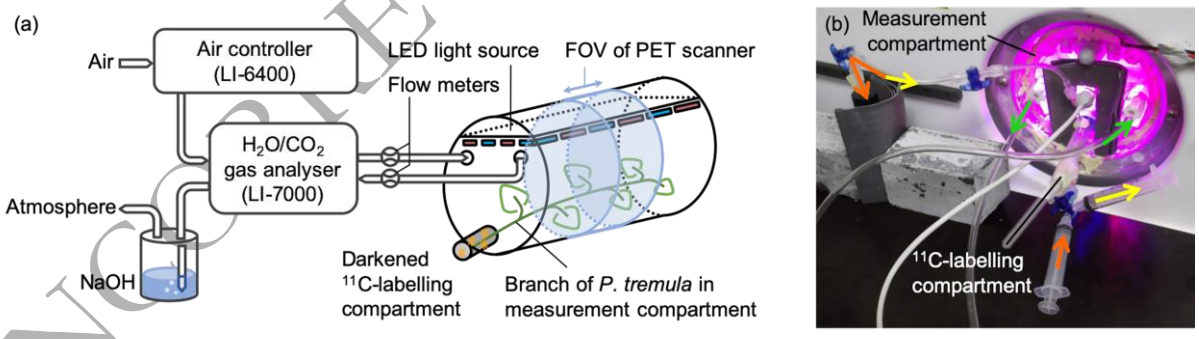

Figure 3 Example of a (a) *P. tremula* branch inside the field-of-view of the PET-scanner and the corresponding (b) static (upper left corner) and dynamic PET images with a temporal resolution of 10 min (timestamp in min shown in the upper left corner of each dynamic PET image). An $^{11}CO_2$-enriched aqueous solution was administered to the cut end of the branch (not shown) and internal transport of the ^{11}C-label was visualised by dynamic PET images. The static PET image has highest resolution and is used for image analysis, i.e. drawing six consecutive ROIs around the branch. These ROIs were applied on the dynamic PET images to obtain tracer concentrations per ROI over time, i.e. TACs. Dash dotted ROIs were not used for image analysis since a petiole originated at that part of the branch. Colours varying from black to red represent no to high tracer as indicated by the colour bar.

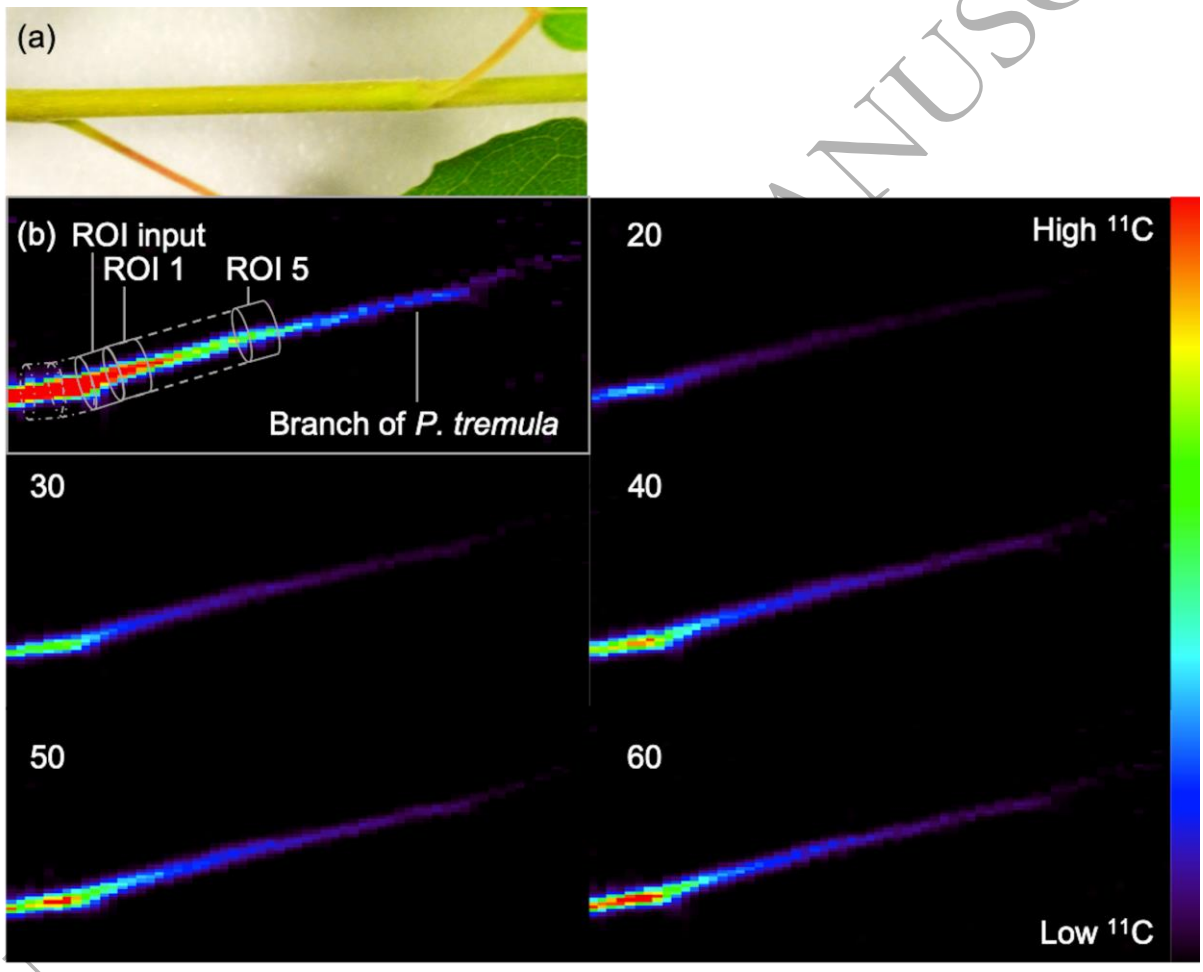

Figure 4 By extracting the tracer concentrations of six consecutive ROIs (ROI input, ROI 1–5) enclosing a branch segment of *P. tremula* on the dynamic PET images in Fig. 3, time-activity curves (TACs) are obtained (circles). The temporal resolution is here 2.5 min and time is expressed in minutes after pulse-labelling aqueous $^{11}CO_2$ to the cut end of the branch. Simulation of the model as in Fig. 3 using the calibrated parameters (i.e. describing the best model fit to the measured TACs) resulted in the simulated TACs (lines). Input ROI measurements are used as input for the compartmental model. Tracer concentrations are expressed in MBq.

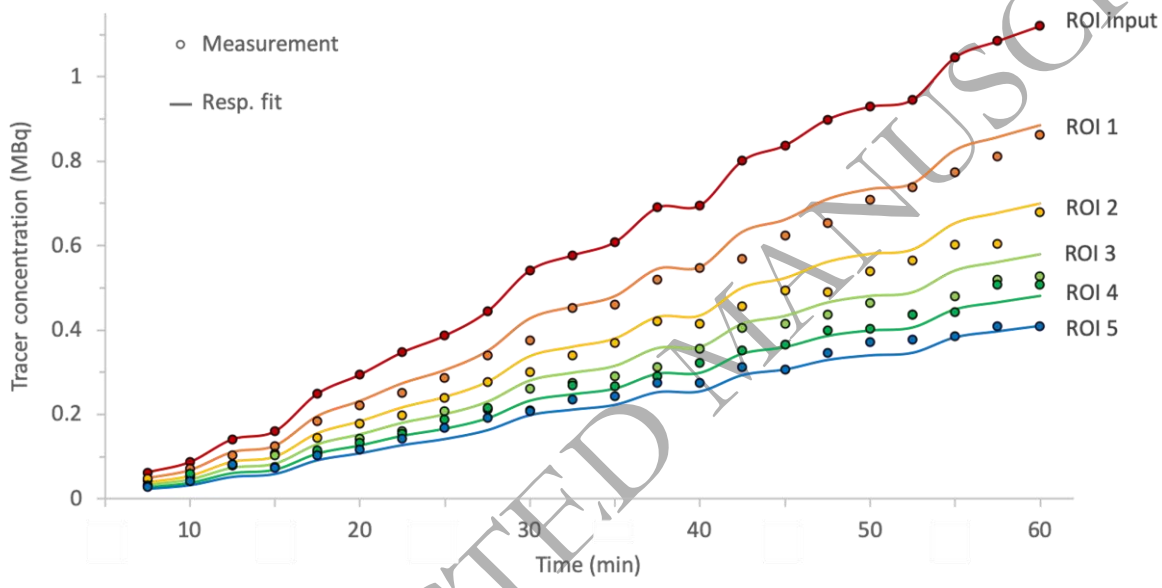

Figure 5 Schematic of the compartmental model used to describe $^{11}CO_2$-tracer movement in six consecutive ROIs (ROI input, ROI 1-5) within a branch segment. The model is described by four parameters, i.e. xylem CO_2 transport speed v_{CO2} (mm min^{-1}) and exchange parameters *a*, *b* and *c* (min^{-1}) as defined by Eqs. (2-5). Through sap flow, $^{11}CO_2$ enters and moves within the xylem (i.e. compartment 1) of each ROI with transport speed v_{CO2}. Within each ROI $^{11}CO_2$ can move from the xylem to surrounding parenchyma and apoplastic spaces (i.e. compartment 2) through *a*. The tracer can subsequently (i) enter compartment 3, via *b*, where it is assimilated by P_{wt} and stored, (ii) exit the ROI and be directed to the atmosphere through *c* or (iii) stay in the second compartment. For each of the ROIs, parameters are assumed equal, and data for the input ROI is directly calculated from measured activity.

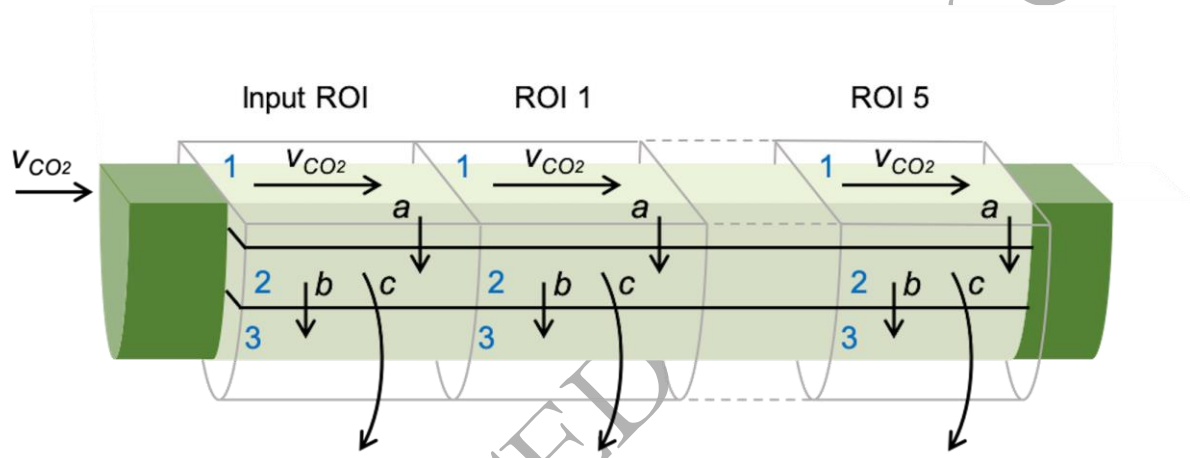

Figure 6 Normalised sum of tracer concentration per ROI over the scanning period of one hour, averaged over all three ^{11}C-experiments performed on branches of *P. tremula* (error bars indicate SE). Tracer concentrations were normalised per experiment with respect to the concentration measured in the input ROI.

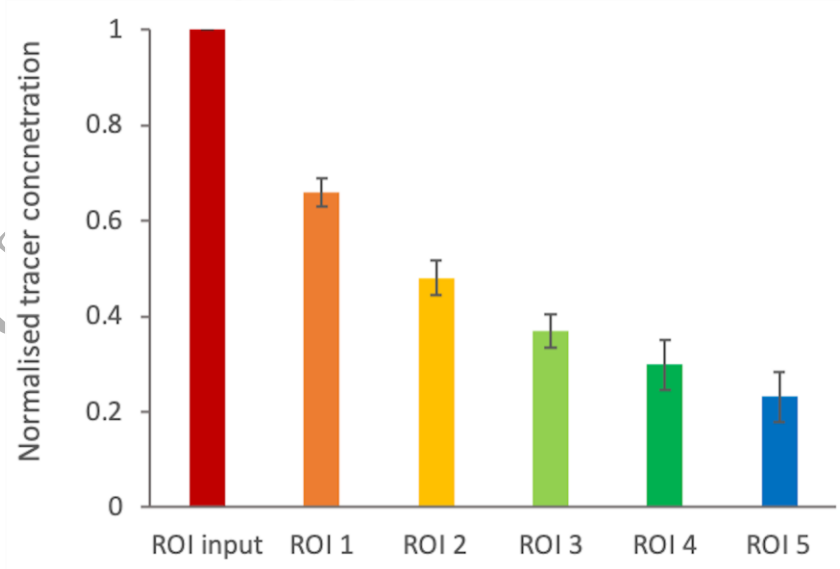

Figure 7 Average estimated parameter values for the compartmental model as defined by Fig. 5, with (a) average PET image-estimation of the transport speed $v^*_{CO_2}$ by means of the distance of an ROI from the cut end of the branch and the time at which the tracer was first detected in that ROI, and average model-estimation v_{CO_2}. No significant difference ($p > 0.05$) was found between both transport speeds (b) Average model parameter estimates *a*, *b* and *c*. Average values were calculated over the experiments performed on branches of *P. tremula* while error bars indicate SE.

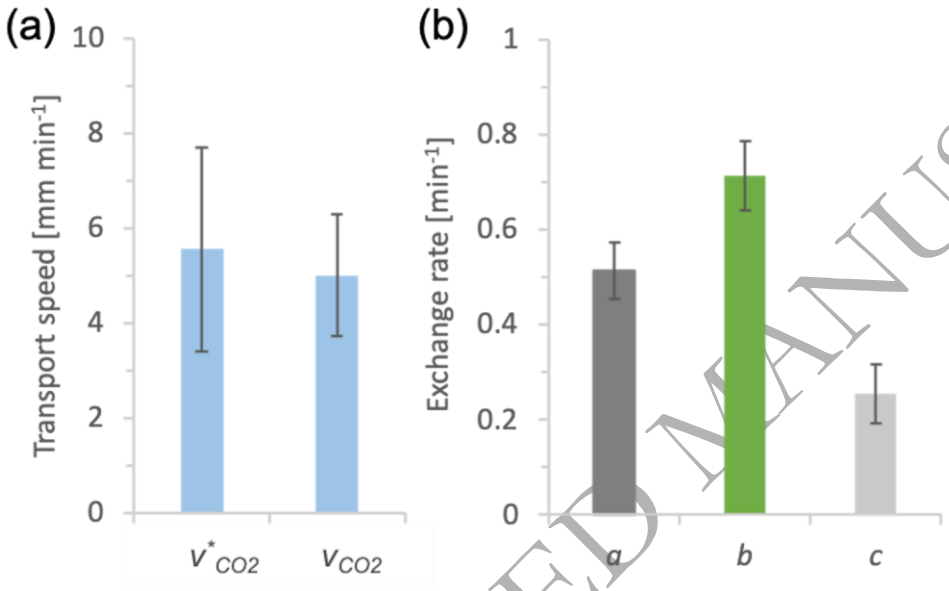

Figure 8 Estimated parameter values for the compartmental model as defined in Fig. 5 (a, b) and the calculated relative carbon fluxes (c), in function of the simulated transport rate of CO_2 within xylem conduits (v_{CO_2}): (a) Relation between the measured leaf transpiration rate and v_{CO_2} (R^2 of 0.71); (b) Relation between exchange parameters (*a*, *b* and *c*) and v_{CO_2} (R^2 of 0.88, 0.79 and 0.71, respectively). Parameters *a*, *b* and *c* represent the tracer fractions between compartments defined by Eqs. (2-4); and (c) Relation between relative carbon fluxes $A_X^{\%}/CO_{2,X}$, $F_T^{\%}/CO_{2,X}$ and $E_A^{\%}/CO_{2,X}$ and v_{CO_2}. Storage flux $\Delta S^{\%}/CO_{2,X}$ was omitted as its values averaged 0.01. Error bars indicate 95% confidence interval and are derived from the uncertainty analysis.

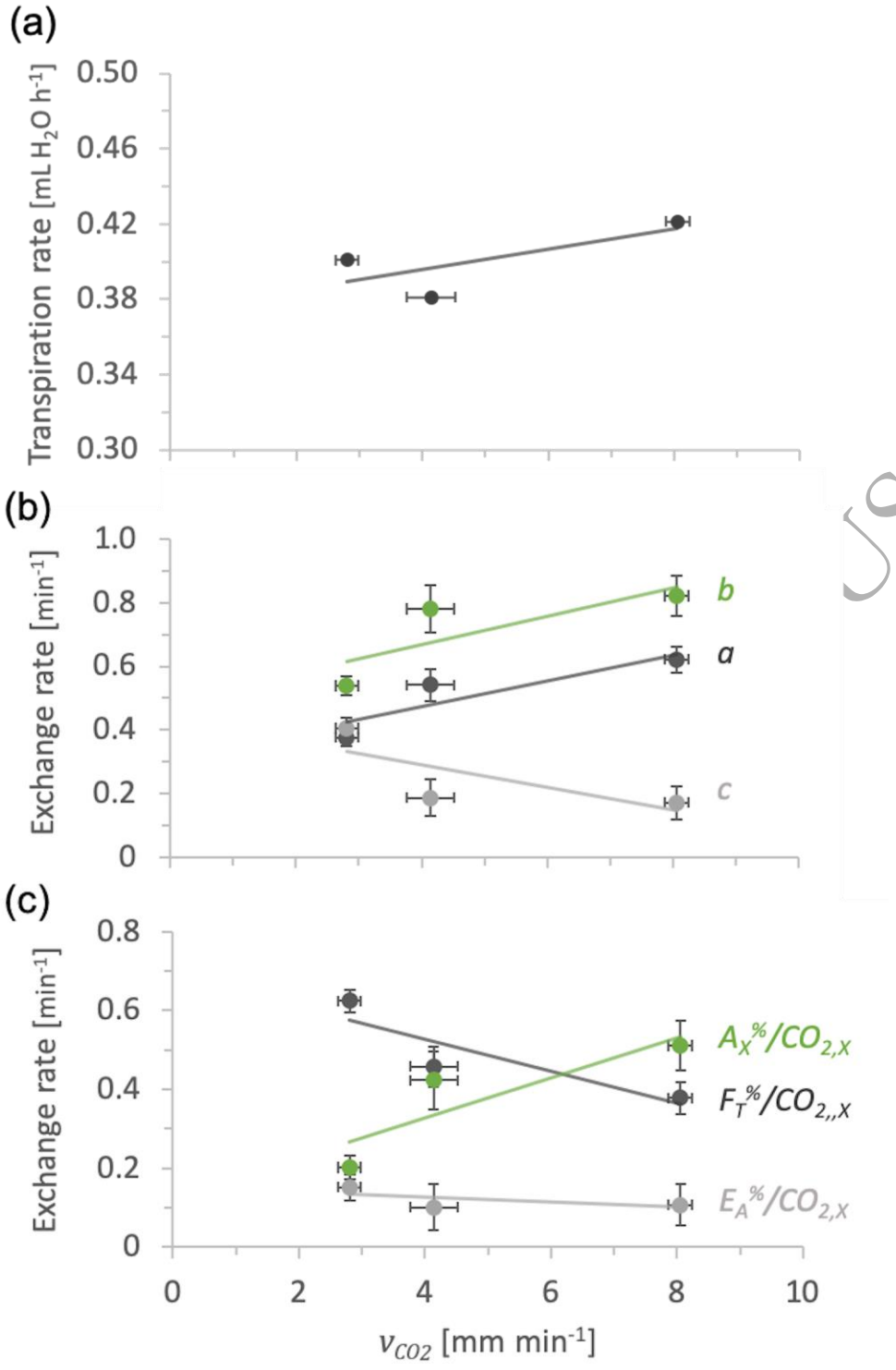

Tables

Table 1: Abbreviations and definition of variables and carbon fluxes in woody tissues.

Abbreviation	Definition
R_S	Stem respiration
E_A	Stem CO_2 efflux to the atmosphere
F_T	CO_2 transport through xylem
ΔS	Storage flux of gaseous CO_2
A_X	Assimilation of $CO_{2,X}$ through P_{wt}
$CO_{2,X}$	Xylem-transported CO_2
P_{wt}	Woody tissue photosynthesis
v_{CO2}	Transport speed of internal CO_2